# Tumour cords and their response to anticancer agents

Alessandro Bertuzzi[1], Antonio Fasano[2], Alberto Gandolfi[1], and Carmela Sinisgalli[1]

[1] Istituto di Analisi dei Sistemi ed Informatica "A. Ruberti" - CNR,
Viale Manzoni 30, 00185 Roma, Italy
bertuzzi@iasi.cnr.it gandolfi@iasi.cnr.it sinisgalli@iasi.cnr.it
[2] Dipartimento di Matematica "U. Dini", Università di Firenze,
Viale Morgagni 67/A, 50134 Firenze, Italy fasano@math.unifi.it

## 1 Introduction

### 1.1 Modelling cords and spheroids

Blood vessels in vascularized tumours are in general irregular and chaotically oriented. However, more ordered structures have been observed, mainly in experimental tumours, where tumour cells proliferating around a blood vessel give rise to approximately axisymmetric aggregates called *tumour cords* [36, 29, 33]. Tumour cords generally differ from each other in size and orientation and, depending on their stage of development and on the way they are organized in space, may or may not be surrounded by a necrotic region. In the presence of necrosis, the mean thickness of a cord is $60 - 130\,\mu$m in different tumours, with mean radius of central vessels of $10 - 40\,\mu$m. Figure 1 shows a schematic cross-section of a system of cords in the absence of necrosis (panel A) or separated by a connected necrotic region (panel B). We have assumed in this figure that blood vessels are parallel, identical and regularly spaced, as in the Krogh model of microcirculation [32]. The assumption of a Krogh-like vasculature allows us to formulate a highly idealized model of a vascular tumour.

The main difficulty in the experimental study of tumour cords is that they cannot be grown *in vitro*. This explains why much more attention, also by mathematicians, has been devoted to the so-called multicellular tumour spheroids, i.e. approximately spherical aggregates of tumour cells which can be easily grown *in vitro* under well controlled conditions (see the review [34] for the experimental issues, and [17, 3] for the mathematical modelling).

From the modelling point of view, the fact that cords receive nutrients from the central blood vessel offers some advantages. For instance, the zone of more intense proliferation can be identified as the innermost region, with

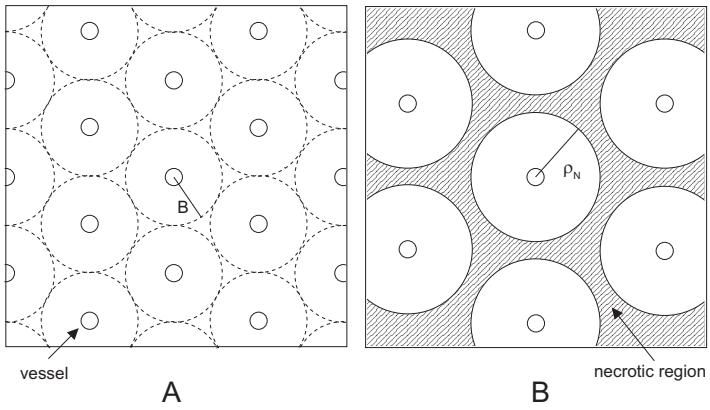


**Fig. 1.** Scheme of an array of tumour cords. Panel A: vessels close enough to provide nutrient supply to all surrounding cells. Panel B: the increased distance among vessels causes peripheral necrosis. Symbols will be explained in section 2.

a progressive weakening of activity toward the periphery, possibly reaching a region of complete necrosis. For avascular tumour nodules receiving nutrients from the surroundings the situation is obviously reversed, but there is no general agreement on how deep in the tumour the cells proliferate. In some models, proliferation is assumed to be allowed only for cells situated in a thin peripheral rim, or even just at the surface of the tumour. This question is particularly important when dealing with the geometrical instability of the tumour (see [26]), that from a slightly perturbed spherical shape may eventually produce finger-like structures. Besides [16], the formation of fractal structures is described in [25] on the basis of a discrete model. We may have an idea of how delicate is the issue of the surface proliferative activity by observing that there are models that concentrate the whole activity on the tumour surface, and assume opposite views about the relative importance of the growth-favouring nutrient concentration and the growth-inhibiting pressure (both higher in tips in a non-spherical shape). Compare for instance the models in [1] and [16], both able to generate complicated shapes by means of different mechanisms.

If we concentrate on modelling the evolution of just one cord in the interior of a more or less regular cohort, the chosen element confines with other similar elements. Thus we do not deal with the problem of how the active surface of a tumour interacts with the surrounding tissue in the body. This subject, however, is receiving growing attention. For instance, it has been suggested that as a byproduct of glucose metabolism an acidic environment can be created. The corresponding pH level can be lethal to the adjacent normal tissue, while tolerated by the tumour cells [35]. Another advantage in modelling cords is

that the cell velocity is known at the inner boundary: cells adhering to the central blood vessel have zero velocity. This information is of great help in integrating the differential equation for the cell velocity (see section 2.2). On the contrary, in spheroids carrying a necrotic core there is no point where the velocity of live cells is known a priori, and information must be retrieved by describing the dynamics of the necrotic core.

That said, there are also questions that turn out to be more complicated in tumour cords than in spheroids. The most evident one is about the geometry. While approximating the spheroid with a sphere is an obvious choice in the framework of the continuum approach, attributing a circular cylindrical shape to a cord is certainly questionable for the reasons already mentioned. Moreover, the concentration of nutrients and the blood pressure change along the cord and restrictions on their relative variations must be imposed. We will briefly discuss this point in section 2.3. The reward of cylindrical symmetry is however remarkable, because this assumption allows to bypass the mechanical problem of the cell-cell and cell-liquid interactions (if we confine ourselves to these two constituents) that determine the cell motion.

A disadvantage of the cylindrical *vs.* the spherical geometry is the higher dimensionality of the dynamics of extracellular fluid, which permeates the whole tumour. The role of the fluid is essential, because it provides the material for the growth of dividing cells. In a sphere we may suppose that the fluid velocity, as well as the cell velocity, is purely radial (we obviously refer to average quantities). In cylindrical tumour cords, it is still reasonable to take a radial velocity field for the cells in a stage in which expansion in the direction of the blood vessel has been completed. On the contrary, the fluid, which comes from the central blood vessel and crosses the whole cord, must eventually leave the cylinder formed by the cord and the peripheral necrosis from the two bases, thus acquiring a velocity with a longitudinal component.

Another difficulty, which is present in modelling tumour cords and is common to modelling of all vascular tumours, is the possibility that internal stresses grow so large to produce the collapse of blood vessels, cutting out nutrients supply. Predicting this event obviously requires the computation of the stress at the blood vessel wall. Studies in this direction have been performed in [15, 2] on the basis of suitable constitutive laws for the mechanical behaviour of the tumour. So far such an analysis has not been performed for tumour cords. Not including the stresses in the model is a strong limitation, not only concerning the blood vessel collapse, but also for the inhibitory action that compression may have on cell proliferation. Such effect has been considered by some authors [18, 20], mainly in the context of models that consider cells and extracellular liquid as two interacting fluids. Radial compression, however, could also be the cumulative result of the traction exerted on the expanding cell layers. We believe that this aspect should receive adequate attention in the future.

Despite all differences between spheroids and tumour cords, they share many features and what is obtained in one context should not be ignored in

the other. One of the most interesting aspects that have been emphasized in modelling tumour cords is that their evolution is constantly accompanied by the presence of *unilateral constraints*, as it will be illustrated later. These constraints should be accounted for also in the evolution of the live cells-necrosis interface in spheroids subjected to treatment.

One more - and last - general remark about modelling of tumour cords, applicable also to spheroids, is about the justification of adopting the continuum approach. This choice may look rather questionable, since a typical cord thickness is of the order of 4–7 cellular diameters (as in many cases is the viable rim in spheroids), thus pointing in favour of a discrete approach. One should not forget, however, that the typical length of a cord is about 30 cellular diameters, so that the number of cells in a cord is of the order of $10^3$. We may take advantage of this fact by selecting the so-called representative elementary volume in the form of a thin cylindrical shell, which despite its small thickness, intersects a sufficiently large number of cells. Thus, basic quantities such as the local volume fraction occupied by cells, acquire a physical relevance.

### 1.2 Modelling treatments

Coming to treatments, we enter a huge subject because there are many different techniques, each presenting peculiar difficulties for mathematical modelling. The ultimate target of the models should be the optimization of the treatment. Let us briefly introduce some of them, restricting to treatments whose effects can be more directly investigated by means of tumour cord modelling.

*Chemotherapy.* A mathematical model should keep into account the way the drug is transported within the tumour and delivered to the cells, the way the drug is taken up and possibly released after cell death, and the modality of the cytotoxic action exerted. Relatively small molecules are mainly transported by diffusion, while advection by extracellular liquid may have an important role for molecules of larger molecular weight. Also, the interaction with cell membrane may decide whether the drug permeates the whole tumour volume or is selectively concentrated in the extracellular liquid. In vascular tumours, the intricacy of the vessel network may be an obstacle to the drug delivery because of the inefficient blood flow [31].

*Radiation.* The short duration of the delivery of a single radiation dose is usually translated into the model by updating the initial conditions. The difficulty here consists in describing the kinds of damage suffered by the cells, taking into account their damage repair ability, and phenomena, such as reoxygenation, that influence the cell population radiosensitivity. Optimizing the intensity and frequency of radiation doses is obviously of great importance, trying not only to maximize the effect on the tumour, but at the same time to keep the damage to the normal tissues at an acceptable level. Models

have been proposed for the spatially homogeneous case and only very recently for tumour cords.

*Antibodies.* Antibodies target specific receptors on the tumour cells. They can be charged with toxins or radio-nuclides. Advection may be important in their transport. We will return to this subject later in the paper.

*Viruses.* Specific viruses able to infect tumour cells, replicate inside them and cause cell lysis, are deployed in the tumour. Some mathematical models have been proposed [40, 27]. Other therapeutic applications under study use viruses as vectors for gene therapy. Due to the size of viruses, diffusion looks negligible but even advection is scarcely efficient, so that transmission takes place mainly by direct infection of neighbouring cells.

In this chapter we shortly review the model for the evolution of tumour cords developed in [7, 8, 9, 10], as well as the attempts of modelling the response to drugs and radiation, and the transport of antibodies able to bind to tumour cell surface antigens [11, 12, 13].

## 2 The basic model for the evolution of tumour cords

A first model of tumour cords was proposed in [5], including the age structure of the cell population, and mathematical aspects of this approach were investigated in [39, 23]. This model was sketched in the review paper [24]. Age structure is essential in many cases, e.g. when studying the distribution of a proliferation marker taken up at a specific phase of the cell cycle [6], but for other purposes age effects can be averaged out. The model described in the following does not include age structure, whereas it includes the diffusion and consumption of the nutrient, the flow of interstitial fluid, and predicts the evolution caused by treatments.

### 2.1 Structure of the cord. Cell and fluid dynamics.

Figure 2 depicts the idealized geometry of a tumour cord surrounded by necrosis. Let $r_0$ denote the blood vessel radius and $\rho_N$ denote the cord radius. In the domain $r_0 < r < \rho_N$, the cell population may be subdivided into proliferating (P), quiescent (Q), and apoptotic cells, all surrounded by extracellular liquid. Such constituents are supposed to have the same mass density, and the corresponding local volume fractions $\nu_P$, $\nu_Q$, $\nu_A$, $\nu_E$ add up to one. The surface $r = \rho_N$ is the interface with the necrotic region, $\rho_N < r < B$. Assuming the cord to be inside an array of parallel and regularly spaced cords, the outer boundary $B$ prevents any mass exchange with the neighbouring cords. Although we will mainly deal with the case of cords surrounded by necrosis, we may also consider the case in which the necrotic region is absent (Fig. 1A). In such a case, $B$ is the cord radius. The longitudinal coordinate $z$ varies in the interval $[-H, +H]$. The liquid, which enters the system at $r = r_0$, leaves from the bases $z = \pm H$.

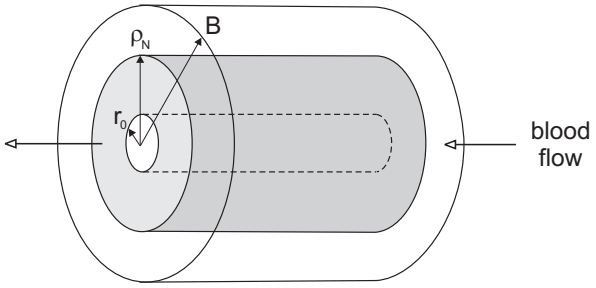


**Fig. 2.** Geometry of the tumour cord (symbols explained in the text).

We assume that cells form a porous medium of *constant* porosity (that is, $\nu_E$ is constant) and, irrespectively of their state, they move with the radial velocity $\mathbf{u} = (u(r,t),\, 0)$. The porosity is thus independent of the stress the cells are experiencing (we also will neglect the possible influence of the stress on the proliferation rate). The assumption that the cord can always be viewed as a packed arrangement of cells, possibly including dead and already degrading cells, limits the applicability of the model to cases in which the cellular component maintains some adhesion and is not severely reduced as a consequence of treatment. Therefore, the model could be significantly improved by including the computation of the stress and the possible degradation of the structure.

The velocity $\mathbf{v}$ of the fluid relative to the cells in the live cord is given by Darcy's law

$$\nu_E(\mathbf{v} - \mathbf{u}) = -\kappa \nabla \tilde{p}\,, \tag{1}$$

where $\kappa$ is the hydraulic conductivity and $\tilde{p}$ is the pressure of the liquid. Dealing with (1) in our case is not simple, in view of the fact that the dynamics of the fluid in the cord is coupled with the dynamics of the fluid in the necrotic region. The rigorous way to proceed would be to take the divergence of both sides in (1) and use the information on $\nabla \cdot \mathbf{v}$, $\nabla \cdot \mathbf{u}$ derived from mass balance, thus obtaining an elliptic equation for $\tilde{p}$ to be associated with complicated interface conditions. We choose instead an approximate description that retains however the most relevant information, that is the total fluid flow across each cylindrical section. This procedure amounts to considering the longitudinal average of the radial component of $\mathbf{v}$. Performing the longitudinal average of $\nabla \cdot \mathbf{v}$, where $\mathbf{v} = (v_r,\, v_z)$, and setting

$$v(r,t) = \frac{1}{2H} \int_{-H}^{H} v_r(r,z,t)\, dz\,,$$

one gets

$$\frac{1}{r}\frac{\partial}{\partial r}(rv) + \frac{1}{2H}[v_z(r,H,t) - v_z(r,-H,t)]\,.$$

The second term expresses the outflow rate from $z = \pm H$, which has to be specified in some way. Our choice is to introduce the longitudinal average of

the pressure,

$$p(r,t) = \frac{1}{2H}\int_{-H}^{H} \tilde{p}(r,z,t)\,dz\,,$$

and to assume that the outflow rate is proportional to the difference $p-p_\infty$. The constant $p_\infty$ is identifiable as a "far field" pressure, namely the pressure in the lymphatic vessels. Thus the quantities utilized in our model are $v(r,t)$, $p(r,t)$. We remark that the difficulties we have emphasized are peculiar to the cord geometry. The averaging procedure is not required in the case of a spheroid.

### 2.2 Mass balance and oxygen dynamics

We are now ready to write down the mass balance equations for the various cell subpopulations

$$\frac{\partial \nu_P}{\partial t} + \frac{1}{r}\frac{\partial}{\partial r}(ru\nu_P) = \chi\nu_P + \gamma\nu_Q - \lambda\nu_P - \mu_P\nu_P\,, \tag{2}$$

$$\frac{\partial \nu_Q}{\partial t} + \frac{1}{r}\frac{\partial}{\partial r}(ru\nu_Q) = -\gamma\nu_Q + \lambda\nu_P - \mu_Q\nu_Q\,, \tag{3}$$

$$\frac{\partial \nu_A}{\partial t} + \frac{1}{r}\frac{\partial}{\partial r}(ru\nu_A) = \mu_P\nu_P + \mu_Q\nu_Q - \mu_A\nu_A\,, \tag{4}$$

and for the liquid

$$\nu_E\nabla\cdot\mathbf{v} = \mu_A\nu_A - \chi\nu_P\,. \tag{5}$$

In the above equations, $\chi$ is the proliferation rate, $\gamma$ and $\lambda$ are the rates of the transition Q→P and, respectively, P→Q, $\mu_P$ and $\mu_Q$ are death rates, $\mu_A$ is the volume loss rate of dead cells. The coefficients $\gamma$ and $\lambda$ are increasing and, respectively, decreasing functions of the oxygen concentration $\sigma(r,t)$; the coefficients $\mu_P$, $\mu_Q$ rather than spontaneous death represent the action of a cytotoxic agent, or can be associated to the damage produced by radiations. Thus, the knowledge of $\mu_P$, $\mu_Q$ relies on the determination of other quantities, whose evolution should also be modelled.

Summing (2)-(4) (remember that $\nu_P+\nu_Q+\nu_A = \nu^\star$ is constant), produces a simple differential equation for $u$:

$$\frac{1}{r}\frac{\partial}{\partial r}(ru) = \frac{1}{\nu^\star}(\chi\nu_P - \mu_A\nu_A)\,.$$

Adding also (5), we get

$$\nabla\cdot(\nu_E\mathbf{v} + (1-\nu_E)\mathbf{u}) = 0\,, \tag{6}$$

that expresses global incompressibility. Taking the longitudinal average of (6) as we have described above, we find

$$\frac{1}{r}\frac{\partial}{\partial r}(rv) = -\frac{1}{\nu_E}\big(\chi\nu_P - \mu_A\nu_A + \frac{\zeta_{out}}{H}(p-p_\infty)\big)\,,$$

where the coefficient $\zeta_{out}$, possibly dependent on $r$, measures the drainage efficiency from the cord ends. Going back to Darcy's law (1), we can now derive its averaged form as

$$\nu_E(v-u) = -\kappa \frac{\partial p}{\partial r}\,,$$

which in our scheme is used to obtain the pressure:

$$p(r,t) = p_0(t) - \frac{\nu_E}{\kappa}\int_{r_0}^{r} [v(r',t) - u(r',t)]\, dr'\,, \tag{7}$$

where the new unknown $p_0(t) = \lim_{r\to r_0^+} p(r,t)$ appears.

We consider the oxygen as the critical "nutrient", although other substances are important for cell energy metabolism, see for instance [19] and the recent paper [38] where oxygen, glucose and lactate concur in determining the level of ATP in the cell. The high permeability of cell membrane to oxygen allows to disregard the difference between extracellular and intracellular concentration. Due to the high diffusivity of oxygen, the quasi-steady diffusion-consumption equation

$$\Delta\sigma = f_P(\sigma)\nu_P + f_Q(\sigma)\nu_Q \tag{8}$$

is assumed to be valid, where the functions $f_P$, $f_Q$ that are related to oxygen consumption are of Michaelis-Menten type. We assume that all cells die if $\sigma$ falls to a threshold value $\sigma_N$.

Before modelling the necrotic region, let us write down the boundary conditions for the equations written so far.

### 2.3 Boundary and initial conditions

As we said, at the vessel wall we may impose

$$u(r_0,t) = 0\,.$$

This condition guarantees that $r = r_0$ is a characteristic for (2)-(4), so that the quantities $\nu_P$, $\nu_Q$, $\nu_A$ do not have to be prescribed there.

Concerning the oxygen, we have:

$$\sigma(r_0,t) = \sigma_b\,,$$

where $\sigma_b$ is the oxygen concentration in blood, taken constant.

For the liquid exchange between blood and tumour tissue, a simple condition is the following:

$$\nu_E v(r_0,t) = \zeta_{in}(p_b - p_0(t))\,,$$

where $p_b$ is the (constant) blood pressure, $p_0$ is the unknown introduced in (7), and $\zeta_{in}$ a coefficient expressing the exchange efficiency. We recall here that the assumption that $\sigma_b$ and $p_b$ are both constant is an approximation because of the occurrence of two competing phenomena. Since oxygen is continuously transferred to the cord, its concentration in blood tends to decrease along the vessel in the direction of blood flow. In order to make the concentration as uniform as possible it is necessary that blood flow is sufficiently rapid, which however requires a high pressure drop. The vessel radius and the size of the cord are crucial in determining whether or not a compromise can be reached. On the basis of perfusion data, it has been checked that for cords of average size the two assumptions may be accepted [9].

Considering the interface $r = \rho_N$, a first condition is the continuity of the averaged pressure:

$$p(\rho_N, t) = p_N(t)\,,$$

where $p_N$ is unknown.

The most delicate conditions are concerned with the oxygen dynamics, because here we find two possible regimens:

(s1) cells enter the necrotic region, that is

$$u(\rho_N(t), t) > \dot{\rho}_N(t)\,, \tag{9}$$

which means that $\sigma$ has reached the necrosis threshold:

$$\sigma(\rho_N(t), t) = \sigma_N\,; \tag{10}$$

(s2) cells do not enter the necrotic region, that is

$$u(\rho_N(t), t) = \dot{\rho}_N(t)\,, \tag{11}$$

while $\sigma$ is free to rise above $\sigma_N$:

$$\sigma(\rho_N(t), t) \geq \sigma_N\,. \tag{12}$$

In both cases, according to the quasi-steady diffusion assumption, we impose

$$\left.\frac{\partial \sigma}{\partial r}\right|_{r=\rho_N(t)} = 0\,.$$

Thus the motion of the interface takes place under two unilateral constraints. Note that (10) actually defines $\rho_N(t)$. Typically the switch from (9)-(10) to (11)-(12) occurs when cells are killed by a treatment, that reduces oxygen consumption and pushes the interface outwards. The interface velocity cannot however exceed the cell velocity, since no living cell can be produced from the necrotic material. The converse switch is instead typical of the tumour regrowth, which, under the conditions (11)-(12) would tend to force $\sigma$ below $\sigma_N$. Simulations performed in [7] show clearly the essential role of these constraints in the evolution of the cord.

In the absence of necrosis, we have to prescribe for $\sigma$ the no-flux conditions at $r = B(t)$. This boundary is now a material surface, and we have $\dot{B} = u(B(t), t)$. Concerning the pressure $p$, we cannot assign its value at $r = B$. Instead we will have there $\partial p/\partial r\big|_{r=B(t)} = 0$.

Prescribing initial conditions is not as simple as it may look like. For instance, when one wants to investigate the effects of treatments it makes sense in many cases to start from the steady state (the steady state problem includes the equations for the necrotic region, still to be written). Finding the equilibrium solution is itself a highly nontrivial problem. All such issues have been discussed in detail [8, 9].

### 2.4 The necrotic region

We recall that the necrotic region occupies the domain $\rho_N(t) < r < B(t)$, $-H < z < H$. The way the forces exerted at $r = B$ enter the evolution of the system depends on the composition of the necrotic region, that contains a fraction of solid material (dead cells retaining some structural integrity) and a fraction of liquid. We have two possible regimens: (n1) the solid is packed in a sufficiently dense way so to withstand the external action; (n2) the surrounding medium acts directly on the liquid. We take the simplifying assumption that both the pressure and the local volume fraction of dead cells are space independent.

The total volume of the necrotic region is

$$V_N = 2H\pi(B^2 - \rho_N^2) \tag{13}$$

and it splits into the sum $V_N^c + V_N^l$ of the solid and of the liquid volume. The evolution of the latter quantities, disregarding the loss of dead cells through $z = \pm H$, is ruled by mass balance:

$$\dot{V}_N^c = 4H\pi\rho_N(1 - \nu_E)[u(\rho_N, t) - \dot{\rho}_N] - \mu_N V_N^c \,, \tag{14}$$

$$\dot{V}_N^l = 4H\pi\rho_N\nu_E[v(\rho_N, t) - \dot{\rho}_N] + \mu_N V_N^c - q_{out}(t) \,, \tag{15}$$

where $\mu_N$ is the rate of conversion of solid to liquid (remember also that $u - \dot{\rho_N} \geq 0$ which implies $V_N^c > 0$), and $q_{out}$ is proportional to the difference $(p_N - p_\infty)$ and to the area of the cross-section $\pi(B^2 - \rho_N^2)$, with the weight $V_N^l/V_N$ i.e. the liquid volume fraction. Thus

$$q_{out} = 2\zeta_{out}^N \frac{V_N^l}{V_N}\pi(B^2 - \rho_N^2)(p_N - p_\infty) \,, \tag{16}$$

where the coefficient $\zeta_{out}^N$ is comparable to $\zeta_{out}/\nu_E$.

The complement to one of $V_N^l/V_N$, that is $V_N^c/V_N$, is subject to the constraint

$$\frac{V_N^c}{V_N} \leq \nu_N^\star \,, \tag{17}$$

with the equality corresponding to regime (n1). Thus, in regime (n1), imposing $\dot{V}_N^c = \nu_N^\star \dot{V}_N$ in (14) yields a differential equation for $B^2$:

$$\frac{d}{dt}(B^2 - \rho_N^2) = 2\frac{1-\nu_E}{\nu_N^\star}\rho_N\big(u(\rho_N,t) - \dot{\rho}_N\big) - \mu_N(B^2 - \rho_N^2)\,. \tag{18}$$

By setting $\dot{V}_N^l = (1-\nu_N^\star)\dot{V}_N$ and $V_N^c = \nu_N^\star V_N$ in (15) gives an expression for $q_{out}$, which defines $p_N$ via (16).

So far we have ignored the stress, but during regime (n1) $p_N$ is required not to exceed the stress that the surrounding material is able to exert on the system. Such a stress may be considered a function of the overall size of the cohort of cords, that is, a function of $B$. Let $\Psi(B)$ denote such a function, increasing with $B$. Thus, the following constraint has to be satisfied during regime (n1):

$$p_N < \Psi(B)\,. \tag{19}$$

Violating the constraint (19) marks the transition to regime (n2), in which the condition $V_N^c = \nu_N^\star V_N$ is replaced by the condition

$$p_N = \Psi(B)\,, \tag{20}$$

and (17) as a strict inequality is present as a new constraint. Now (14) can be integrated, providing $V_N^c$ as a functional of $\rho_N$ and $u$, while the combination of (13), (15), (16), (20) leads to the differential equation for $B$ replacing (18). This picture of the necrotic region is the one proposed in [10].

In the formation of a spheroidal tumour the early stage of the necrotic core will be under the regime (n1). The same is true for the first appearance of a necrotic zone around the cord. However, predicting in a more precise way the transition to the other regime would require a definition of the age of the outer rim of the necrotic region around the viable core (or of the inner core in the case of the spheroid), abandoning the simple model of the homogeneous mixture.

We conclude this section by recalling that the well-posedness of the model was investigated in [8, 9], including the analysis of the steady state in the case of untreated tumour. Useless to say, the presence of constraints in the dynamical case produces serious mathematical difficulties.

## 3 Response of cords to treatments

The model illustrated in the previous section has been applied to study the response of cords to various types of treatment. Here we comment the work done in this direction. Although the results give several interesting clues on the effects of treatments, we must say that they are far from being conclusive. One of the reasons is that the model used, despite the many details it contains, does not give a full description of the tumour.

### 3.1 Treatments by drugs

Already in [7], where the model was first presented in a version not including the dynamics of the fluid, the effect of a cytotoxic drug was considered. That model was only applicable to drugs whose transport mechanism is mainly diffusive. We estimated that advective transport is indeed negligible if diffusivity is not less than $5\times10^{-8}$ cm$^2$/s, a condition satisfied by many anticancer drugs. Moreover the drug was supposed to diffuse the same way in the liquid and in the cells. The cell death rate was taken as a given function of the drug concentration $c$. Of course the diffusion equation for $c$ contains a sink term, expressing drug uptake and consumption by the cells, which vanishes in the necrotic region. The value of $c$ was prescribed at the blood vessel wall as a function of time, following drug administration, while zero flux was prescribed at the boundary $r = B(t)$.

The effect of cell killing on the evolution of the cord, including the distribution of pressure and the change experienced by the necrotic zone, was investigated (in the context of the full model illustrated in section 2) in [10]. However, instead of examining the dynamics of the drug, the death rates $\mu_P$, $\mu_Q$ were chosen as a combination of space independent functions decaying exponentially with time, so to reproduce the *expected* effect of the delivery of a bolus dose. Namely, we chose [10, 11]:

$$\mu_P(t) = \frac{m_P}{\tau_1 - \tau_2}(\mathrm{e}^{-t/\tau_1} - \mathrm{e}^{-t/\tau_2}),$$
$$\mu_Q(t) = \frac{m_Q}{\tau_1 - \tau_2}(\mathrm{e}^{-t/\tau_1} - \mathrm{e}^{-t/\tau_2}),$$

where $\tau_1$ is related to drug removal and $\tau_2$ to the drug distribution in the body compartments.

This shortcut made the simulation simpler, and allowed us to reach some significant qualitative conclusion. For instance it was pointed out that cell killing alone is not enough to produce a marked reduction of the overall size of the tumour, but it must be accompanied by an effective drainage of the liquid (meaning a sufficiently high value of the coefficients $\zeta_{out}$, $\zeta^N_{out}$ of the model). Figure 3 shows an example of the time evolution of the cord in the case of a cycle-specific drug, that is, a drug affecting mainly the proliferating cells ($m_P > m_Q$). Panel A reports the ratio between the total volume (per unit cord length) of viable cells and its value at $t=0$, describing the dynamics of the viable cell population following the treatment. The reduction of the number of viable cells lowers oxygen consumption and thus causes reoxygenation of the cord as shown by the time course of mean oxygen concentration (panel B). The increase in oxygen concentration induces a recruitment of quiescent cells into proliferation, as seen in panel A, so that a transient phase in which the proliferating fraction is higher than the initial one may occur. The radius $\rho_N$ shows an initial shrinkage followed by a regrowth leading to the steady state (panel C). Very soon after the rise of drug concentration the interface

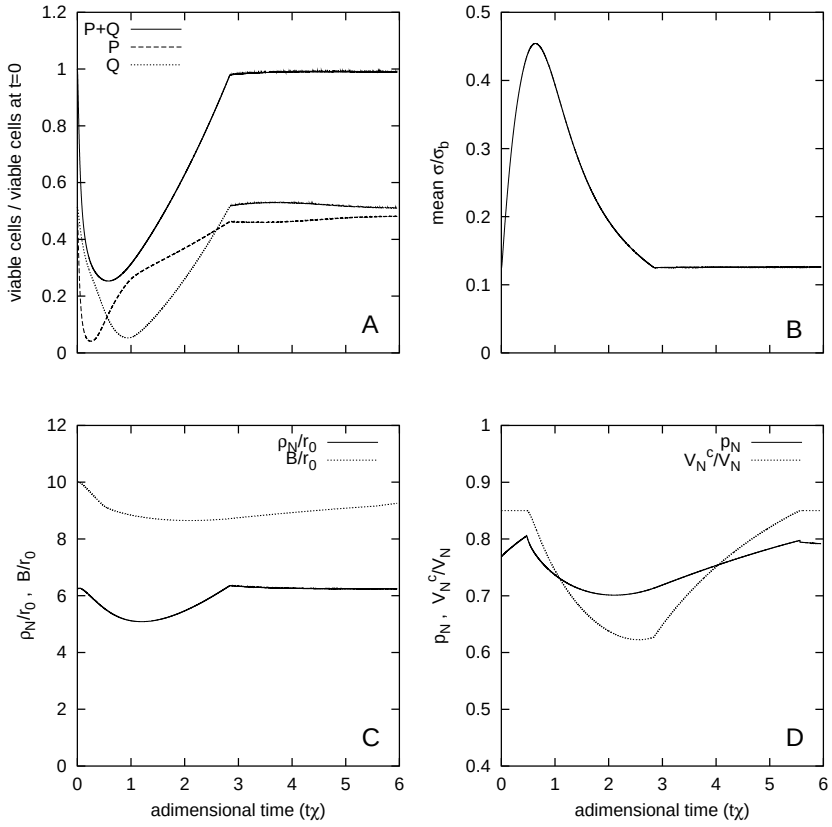


**Fig. 3.** Panel A: time course of the viable cell subpopulations after a single-dose treatment; P proliferating cells, Q quiescent cells. Panel B: mean oxygen concentration. Panel C: cord radius $\rho_N$ and outer boundary $B$. Panel D: pressure and cell fraction in the necrotic region. Parameters as in [24] with $m_P/m_Q = 5$.

$r = \rho_N$ becomes a material surface (see section 2.3). The slope discontinuity that occurs later marks the switching of the interface from the material to the nonmaterial nature. In the same panel, the time course of the boundary $B$ is plotted. Panel D shows the time evolution of the pressure $p_N$ and of the cellular fraction in the necrotic region. In the initial state the constraint (17) is satisfied with the equality sign and the pressure is less than $\Psi(B)$. Due to the enhanced influx of liquid caused by cell death, $p_N$ increases reaching $\Psi(B)$. At this point the regime changes, $p_N$ is given by $\Psi(B)$ and the cellular fraction goes below $\nu_N^\star$. During the cord regrowth, the influx of liquid decreases and the system switches again to the regime characterized by a cellular fraction equal to $\nu_N^\star$. It was found that the time evolution of the average interstitial pressure in the viable cord closely follows the pressure in the necrotic region because of the high value of Darcy's conductivity.

This numerical experiment opened the way to the mathematical investigation of another question of great interest: what is the effect of splitting a dose of drug? We have considered the case of splitting the dose into two equal boluses spaced by a time interval $T$, and found the splitting advantageous if the sensitivity of the cell population to the drug significantly increases when the oxygen level increases [11]. Comparison between the single dose and the split dose was made by using the survival ratio defined as:

$$\mathrm{SR} = \frac{\min(\text{viable cell volume})_2}{\min(\text{viable cell volume})_1}\,, \tag{21}$$

where the subscripts 1,2 refer to the single and to the split dose, respectively.

A crucial role is played by the ratio $m_P/m_Q$. To understand how dose splitting can enhance the cell killing, one should go back to equations (2)-(3), in which the coefficients $\gamma$, $\lambda$ regulating the transitions $\mathrm{P} \rightleftarrows \mathrm{Q}$ are monotonically dependent (in opposite ways) on the oxygen concentration $\sigma$. As shown by Fig. 3B, when the first half-dose kills a certain fraction of cells, oxygen concentration increases favouring the transition of the surviving Q-cells to the P-state. Then, if the ratio $m_P/m_Q$ is large, the "upgraded" cells will have a much greater chance to be killed by the application of the second half-dose. This phenomenon is called *resensitization*. Figure 4, left panel, shows the behaviour of SR as a function of the inter-fraction interval, when using different values for $m_P$, $m_Q$. Of course, taking $m_P/m_Q = 1$ eliminates resensitization completely, while a ratio $m_P/m_Q = 5$ shows a marked effect of the dose splitting procedure. The figure also shows the existence of an optimal choice of the splitting time, corresponding to the time in which the ratio between P and Q cells is maximal. These results are obviously qualitative, but they strongly suggest to promote experimental research in this direction.

Dose splitting is an interesting topic also in the context of radiation therapy [14], as we will see in the following section.

### 3.2 Response to impulsive irradiation

#### A spatially uniform model

Radiations can produce cell damages which may later lead to cell death either by a direct action or as a consequence of a misrepair process. In order to understand and to model the latter mechanism, suppose that the DNA double strand is broken by radiation at one point. This damage has a certain probability of being repaired, thus allowing the cell to survive. However, along with the repair consisting in joining the two segments of the same DNA molecule, there can also be "cross-repairs" in which two segments originally belonging to different strands are joined, giving rise to two misrepaired strands. The outcome of such mixing may, or may not, be lethal for the cell. Each DNA double strand has a specific point, known as its centromere, acting as a pivotal center during mitosis. Now, the "cross-repair" can produce two chromosomes

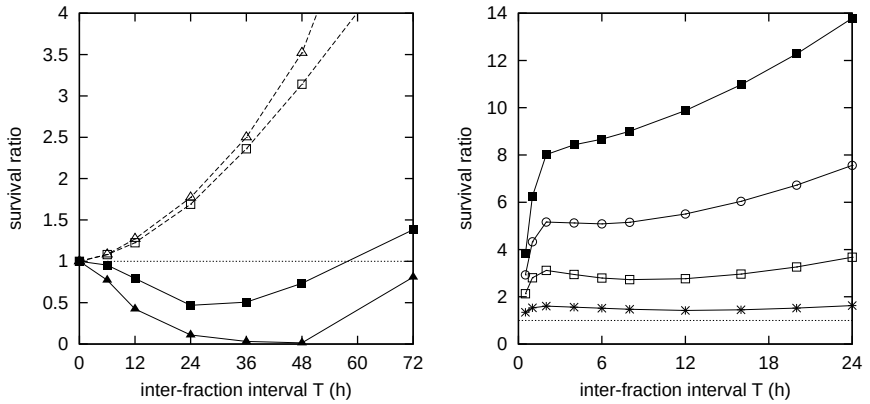


**Fig. 4.** Survival ratio as a function of the time interval between the two fractions. Left panel: SR for split-dose drug delivery. Closed symbols: $m_P/m_Q = 5$; $m_P = 4$ for each fraction (squares), $m_P = 8$ (triangles). Open symbols: $m_P/m_Q = 1$; $m_P = 2$ (squares), $m_P = 4$ (triangles). Other parameter values given in [11]. Right panel: SR for split-dose radiation delivery. Effect of the intervessel distance on the survival ratio. Closed squares, $B(0) = 80\,\mu$m; open circles, $B(0) = 90\,\mu$m; open squares, $B(0) = 100\,\mu$m; stars, cord surrounded by necrosis ($\rho_N = 124.75\,\mu$m). Other parameter values given in [13].

with one centromere each, or one with two centromeres and one with no centromere. The occurrence of the latter kind of misrepair produces cells unable to replicate and destined to death. Lethally damaged cells are called "clonogenically dead". Other types of lethal misrepairs can be accounted for in the direct action.

A simple spatially-homogeneous differential model describing the repair-misrepair process was proposed in [22, 30] and can be written as

$$\frac{dN}{dt} = -[\alpha\dot{D} + \frac{1}{2}kU^2]N\,, \tag{22}$$

$$\frac{dU}{dt} = \delta\dot{D} - \omega U - 2kU^2\,, \tag{23}$$

where $N$ is the number of viable cells, $\dot{D}$ the radiation dose rate, $U$ the mean number of DNA double strand breaks per cell (DSB). The term $\omega U$ represents the rate of correct repairs, the term $kU^2$ is the rate of binary cross-repairs, which on one hand eliminate two DSBs each, and on the other have a probability 1/2 of ending up with a lethal damage. Direct lethal action of radiation is represented by the term $-\alpha\dot{D}$, whereas $\delta\dot{D}$ is the rate of DSB production per cell. Cells carrying DSBs are counted in $N$ as long as they do not become lethally damaged.

The duration of pulse irradiation is usually so short that the direct action of radiation and the DSB production can be described simply by setting the

initial conditions for $N$ and for $U$:

$$N(0^+) = N(0^-)\,\mathrm{e}^{-\alpha D}$$
$$U(0^+) = U(0^-) + \delta D\,, \qquad U(0^-) = 0\,,$$

where $D$ is the radiation dose. The solution of (22)-(23) with the above initial conditions provides, in the limit $t \to \infty$, the surviving fraction $S{=}N(\infty)/N(0^-)$:

$$\ln S = -\alpha D + \frac{\omega}{8k}\Big[\ln\Big(1 + \frac{2k\delta D}{\omega}\Big) - \frac{2k\delta D}{\omega}\Big]\,.$$

For $2k\delta D/\omega \ll 1$, which corresponds to neglecting the quadratic term in (23), we obtain

$$S = \exp\Big[-\alpha D - \frac{k(\delta D)^2}{4\omega}\Big]\,. \tag{24}$$

Defining $\beta = k\delta^2/(4\omega)$, we recognize in (24) the so-called linear-quadratic (LQ) model previously proposed on empirical bases [37].

When the dose $D$ is split into two fractions $D/2$, given with an interval $T$, (22)-(23) still allow to evaluate the surviving fraction (after the second dose). For simplicity we just report the new value of $S$ in the case $k\delta D/\omega \ll 1$:

$$S_{\rm split} = \exp\Big[-\alpha D - \beta\frac{1+\mathrm{e}^{-\omega T}}{2}D^2\Big]\,. \tag{25}$$

Clearly

$$\frac{S_{\rm split}}{S} = \exp\Big[\beta\frac{1-\mathrm{e}^{-\omega T}}{2}D^2\Big] > 1\,, \tag{26}$$

showing that, according to this theory, splitting the dose is never advantageous in terms of cell killing. We can also see that by splitting $D$ into $hD$ and $(1{-}h)D$, the factor $(1{+}\mathrm{e}^{-\omega T})/2$ in (25) is replaced with $2h(h{-}1)(1{-}\mathrm{e}^{-\omega T}){+}1$, showing that the above ratio is maximum for $h{=}1/2$.

However, the analysis sketched above ignores the dynamics of the tumour and, in particular, the possible reoxygenation of the tumour following the first dose as experimentally observed [21]. It must be stressed that the parameters $\alpha$, $\delta$ are increasing functions of the oxygen concentration [41].

### Effects of radiation on a tumour cord

In [13] we studied the dose splitting effect on the basis of the following tumour cord model:

$$\frac{\partial \nu_P}{\partial t} + \frac{1}{r}\frac{\partial}{\partial r}(ru\nu_P) = \chi\nu_P + \gamma\nu_Q - \lambda\nu_P - m_P(r,t)\nu_P\,, \tag{27}$$
$$\frac{\partial \nu_Q}{\partial t} + \frac{1}{r}\frac{\partial}{\partial r}(ru\nu_Q) = -\gamma\nu_Q + \lambda\nu_P - m_Q(r,t)\nu_Q\,, \tag{28}$$
$$\frac{\partial \nu^\dagger}{\partial t} + \frac{1}{r}\frac{\partial}{\partial r}(ru\nu^\dagger) = m_P(r,t)\nu_P + m_Q(r,t)\nu_Q - \mu\nu^\dagger\,, \tag{29}$$
$$\frac{\partial \nu_A}{\partial t} + \frac{1}{r}\frac{\partial}{\partial r}(ru\nu_A) = \mu\nu^\dagger - \mu_A\nu_A\,, \tag{30}$$

where $\nu_P$, $\nu_Q$, and $\nu_A$ have the same meaning as in the basic model of section 2, and $\nu^\dagger$ is the volume fraction of lethally damaged cells. The rates $m_P$ and $m_Q$ represent the effect of the misrepair process that induces lethal damage, $\mu$ is the death rate of lethally damaged cells.

In view of (22)-(23) for the kinetics of DSB repair/misrepair, for the rates $m_P$ and $m_Q$ we assume

$$m_P(r,t) = \frac{1}{2}kX_P^2(r,t)\,, \quad m_Q(r,t) = \frac{1}{2}kX_Q^2(r,t)\,, \tag{31}$$

where $X_P(r,t)$ and $X_Q(r,t)$ denote the mean number of DSBs in an "equivalent" P cell and, respectively, Q cell at the position $r$ at time $t$. These quantities, as derived in [13], satisfy the following equations:

$$\frac{\partial X_P}{\partial t} + u\frac{\partial X_P}{\partial r} = -\omega X_P - 2kX_P^2\,, \tag{32}$$

$$\frac{\partial X_Q}{\partial t} + u\frac{\partial X_Q}{\partial r} = -\omega X_Q - 2kX_Q^2\,. \tag{33}$$

The assumption that all cellular volume fractions in (27)-(30) sum up to a constant $\nu^\star$ yields the equation for the common cellular velocity $u$, as seen in section 2. The dynamics of the interstitial liquid is here of less importance and is disregarded.

If a sequence of impulsive irradiations is given with dose $D_k$ at time $t_k$, $k = 1, 2, \ldots$, $t_1 = 0$, we have the following conditions:

$$\begin{aligned}
&\nu_i(r,t_k^+) = \nu_i(r,t_k^-)\exp[-\alpha_i(\sigma(r,t_k^-))D_k]\,, \qquad i = P,Q\,,\\
&\nu^\dagger(r,t_k^+) = \nu^\dagger(r,t_k^-) + \sum\nolimits_{i=P,Q}\left(\nu_i(r,t_k^-) - \nu_i(r,t_k^+)\right),\\
&X_i(r,t_k^+) = X_i(r,t_k^-) + \delta_i(\sigma(r,t_k^-))D_k\,, \qquad i = P,Q\,,
\end{aligned}$$

that define the initial data for the differential system (27)-(33) by setting $\nu_i(r,0^-) = \nu_{i0}(r)$, $\nu^\dagger(r,0^-) = 0$, $X_i(r,0^-) = 0$, $i = P,Q$, and the data update at the subsequent delivery times. We have allowed the sensitivity parameters $\alpha_i$, $\delta_i$ to depend on the oxygen concentration according to experimental evidence [41]. Oxygen concentration satisfies the free boundary problem described in section 2, in which in (8) the absorption term due to the population $\nu^\dagger$ must be added.

The model was simulated [13] under different conditions to elucidate the influence of reoxygenation on the split-dose response compared with the response to the undivided dose. Figure 4, right panel, shows the pattern of the survival ratio defined by (21) for three different values of the radius $B$ at $t = 0$ in the absence of necrosis (i.e., for different intervessel distances, see Fig. 1A). In addition, the response of a cord surrounded by necrosis is also shown. When $B$ increases, the whole SR curve is lowered and reaches a minimum in the case of necrosis. This is explained by considering that the mean oxygen concentration decreases as $B$ increases and therefore the average $\beta$ value decreases.

Smaller $\beta$ values, according to the LQ model, are expected to produce smaller SR values (see (26)). Moreover, if the cord radius is small, the reoxygenation induces only a small increase in radiosensitivity because the initial mean oxygen concentration is high, with $\sigma$ falling in the saturating portion of the $\alpha(\sigma)$ and $\delta(\sigma)$ curves. At the higher values of $B$, the SR curve shows an appreciable relative minimum due to the reoxygenation of the cell population that makes the second dose more effective. The initial rising branch of the curve corresponds to the repair process, whose duration is proportional to $1/\omega$. The increase for large $T$ is due to the regrowth of surviving cells between the two doses.

On the basis of the results shown in Fig. 4, we can conclude that the enhancing effect of reoxygenation on cell killing, which was emphasized for drug treatments, is present here too, although it is not strong enough to reduce the survival ratio below the unity. This apparently negative situation can however prove advantageous since the increase of the survival ratio upon splitting may be higher for the normal tissue than for the tumour [13]. Therefore repeated treatments with fractionated doses may lead to a more selective destruction of the tumour mass.

### 3.3 Transport of monoclonal antibodies

Specific antibodies may bind to antigens on the tumour cell membrane. This property can be exploited to deliver a killing agent to the targeted cell (a toxin or a radionuclide [4]). In some cases antibodies can directly exert a cytotoxic action. As a preliminary analysis to the study of tumour therapies based on the use of antibodies, in the paper [12] we have examined the problem of their transport through a cord that has reached a steady state, without considering any cytotoxic action. The scheme that follows may be the basis for a further study.

We consider monoclonal IgG antibodies with two equivalent binding sites. The antigens are uniformly distributed on the cell membrane and are monovalent. Thus the antibodies can be found in three states: (i) free in the extracellular liquid with concentration $c$, (ii) monovalently bound with surface concentration $\hat{b}_1$, (iii) bivalently bound with surface concentration $\hat{b}_2$. All concentrations are supposed to be independent of the longitudinal coordinate $z$. We schematize antigens as receptors with surface concentration $\hat{S}$, and we denote by $\eta^\star$ the ratio of total cellular surface per unit volume to extracellular volume fraction. Consistent with the assumption that the volume fraction occupied by cells in the cord is constant, $\eta^\star$ is a known constant. The formation of bonds is a reversible process, and the formation of double bonds is taken as a sequential process. We introduce the following rate constants: $2k_a$ for the formation of the first bond, $k'_a$ for the formation of the second bond, and $k_d$ for the dissociation of a bond.

That said, after performing the longitudinal mean, the dynamics of the antibodies in the cord is described by the following system [12]:

$$\frac{\partial c}{\partial t} - \frac{D}{r}\frac{\partial}{\partial r}(r\frac{\partial c}{\partial r}) + fv(r)\frac{\partial c}{\partial r} = f\chi\frac{\nu_P(r)}{1-\nu^\star}c - 2k_a\eta^\star c\hat{s} + k_d\eta^\star\hat{b}_1\,, \quad (34)$$

$$\frac{\partial \hat{b}_1}{\partial t} + u(r)\frac{\partial \hat{b}_1}{\partial r} = -\chi\frac{\nu_P(r)}{\nu^\star}\hat{b}_1 + 2k_a c\hat{s} - k_d\hat{b}_1 - k'_a\hat{s}\hat{b}_1 + 2k_d\hat{b}_2\,, \quad (35)$$

$$\frac{\partial \hat{b}_2}{\partial t} + u(r)\frac{\partial \hat{b}_2}{\partial r} = -\chi\frac{\nu_P(r)}{\nu^\star}\hat{b}_2 + k'_a\hat{s}\hat{b}_1 - 2k_d\hat{b}_2\,, \quad (36)$$

with

$$\hat{s} = \hat{S} - \hat{b}_1 - 2\hat{b}_2\,.$$

Here, $u$, $v$, and $\nu_P$ are functions of the radial distance only because the cord is at the steady state. The velocities $u$, $v$ and the size of the cord are provided by the solution of the steady state version of the model in section 2 (with $\mu_P = \mu_Q = 0$, $\nu_A = 0$). In equation (34) we have considered that the transport of antibodies takes place through diffusion (with diffusivity $D$) and advection (with retardation factor $f < 1$).

For the flux of antibodies at the blood vessel wall, once the concentration of antibodies in blood $c_b(t)$ is prescribed, we assume the expression

$$-D\frac{\partial c}{\partial r}\bigg|_{r=r_0} + fv(r_0)c(r_0,t) = \frac{P}{\nu_E}(c_b(t) - c(r_0,t))\frac{\mathrm{Pe}}{\mathrm{e}^{\mathrm{Pe}}-1} + v(r_0)(1-\sigma_f)c_b(t)\,,$$

with Pe (Peclet number) given by $\mathrm{Pe} = \nu_E v(r_0)(1-\sigma_f)/P$, where $P$ is the permeability of the vessel wall, and $\sigma_f$ is the filtration reflection coefficient. No condition is required for $\hat{b}_1$, $\hat{b}_2$ at $r = r_0$, since $u(r_0) = 0$. At $t = 0$ all the unknown concentrations are taken to be zero. The second boundary condition for $c$ requires the description of the antibody transport in the necrotic region.

In the necrotic region, little is known about the interaction of antibodies with degrading cells. Here we suppose that the antigens are retained on the surface of dead cells and are destroyed after cell degradation. Concerning the antibodies bound to cells entering the necrotic region, we suppose that upon cell degradation either (i) antibodies are lost, or (ii) antibodies are set free. Of course these are opposite options describing two extreme situations. They are supposed to provide bounds to the real behaviour which will be somehow in between. Whatever model is chosen, we have to write down the evolution equations for $c$, $\hat{b}_1$, $\hat{b}_2$ and this requires the knowledge of the fields $u(r)$, $v(r)$ also in the necrotic region. A derivation of these quantities is provided in [12], and it is not reported here for the sake of brevity. In that paper, the same approach of section 2.4 has been followed to determine the outer boundary $r = B$ and the necrotic pressure $p_N$.

Once determined the global equilibrium solution for the cord plus the necrotic region, it is possible to write the evolution equations for $c$, $\hat{b}_1$, $\hat{b}_2$ in the necrotic region, which in case (i) take the form

$$\frac{\partial c}{\partial t} - \frac{D}{r}\frac{\partial}{\partial r}(r\frac{\partial c}{\partial r}) + fv(r)\frac{\partial c}{\partial r} = -f\mu_N\frac{\nu_N}{1-\nu_N}c - 2k_a\eta_N c\hat{s} + k_d\eta_N\hat{b}_1\,, \quad (37)$$

$$\frac{\partial \hat{b}_1}{\partial t} + u(r)\frac{\partial \hat{b}_1}{\partial r} = 2k_a c\hat{s} - k_d\hat{b}_1 - k'_a\hat{s}\hat{b}_1 + 2k_d\hat{b}_2\,, \tag{38}$$

$$\frac{\partial \hat{b}_2}{\partial t} + u(r)\frac{\partial \hat{b}_2}{\partial r} = k'_a\hat{s}\hat{b}_1 - 2k_d\hat{b}_2\,, \tag{39}$$

where $\nu_N = V_N^c/V_N$ is the volume fraction of dead cells and $\eta_N$ is the ratio of the cellular surface per unit volume in the necrotic region to the extracellular volume fraction $1-\nu_N$. In case (ii), the term $\mu_N\eta_N(\hat{b}_1+\hat{b}_2)$ must be added to the r.h.s. of (37).

The conditions at the necrotic interface $r=\rho_N$ are: the continuity of $c$; the continuity of the flux of antibodies which, in view of the mass flux continuity, and supposing that the factor $f$ is also continuous, takes the form

$$(1-\nu_N)\frac{\partial c}{\partial r}\bigg|_{r=\rho_N^+} = (1-\nu^\star)\frac{\partial c}{\partial r}\bigg|_{r=\rho_N^-}\,;$$

the continuity of $\hat{b}_1$, $\hat{b}_2$. Finally we have no flux at the outer boundary $B$:

$$\frac{\partial c}{\partial r}\bigg|_{r=B} = 0\,.$$

Numerical simulations have been performed for the input data given by:

$$c_b(t) = c_{b0}\big(m\mathrm{e}^{-t/\tau_1} + (1-m)\mathrm{e}^{-t/\tau_2}\big)\,,$$

with values of $m$, $\tau_1$ and $\tau_2$ as in [28], and are illustrated in Fig. 5. Figure 5 shows the evolution of free and bound antibody for different values of the parameters $k_a = k'_a$ and $k_d$. As expected, the affinity parameter $K = k_a/k_d$ plays an important role: for $K=50$ (left panel) antibodies are mainly present in the doubly bound state while, for $K=2$ (right panel), $\hat{b}_1$ and $\hat{b}_2$ are much closer to each other. In the simulated cases the concentration of free antibodies decays very strongly with the radial distance: this is a clinically interesting information, since it says that the injected antibodies basically do not leave the cord, thus causing no harm to the surrounding tissue. Moreover, we observe that the high binding to cell surface antigens results in a "barrier" to antibody penetration generating a more heterogeneous antibody distribution due to the preferential binding in the inner region of the cord. A comparison between the options (i) and (ii) showed that the fate of antibodies after cell degradation is not particularly important apart from cases in which both the degradation rate of dead cells and the binding affinity are large.

## 4 Conclusions

With reference to an array of tumour cords, taken as a paradigm of a vascular tumour, we have reviewed some models describing the action of treatments.

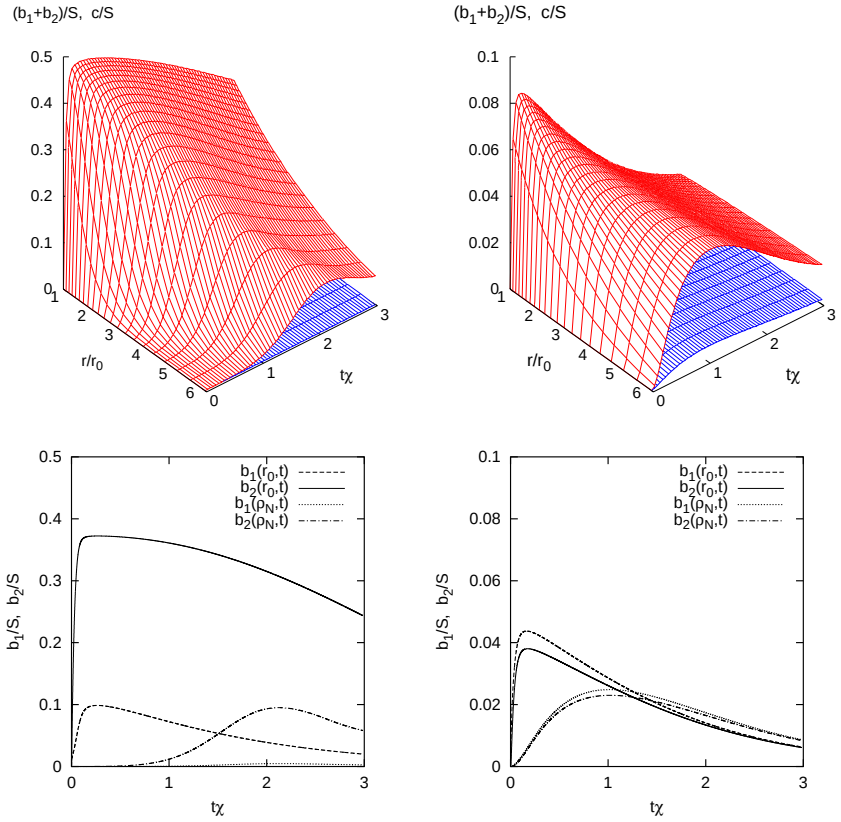


**Fig. 5.** Upper panels: distribution of bound and free antibodies (in both panels the lower surface represents free antibodies). The concentrations reported are normalized. Lower panels: time course of $b_1$ and $b_2$ at $r = r_0$ and $r = \rho_N$. Left panels: $k_a = k'_a = 1000$, $k_d = 20$; right panels: $k_a = k'_a = 100$, $k_d = 50$ (nondimensional units). Other parameters given in [12].

Three classes of treatments have been considered: chemotherapy, radiotherapy, and treatments using antibodies. We have tried to emphasize both the clinical interest of the results obtained and the limitations accompanying the corresponding mathematical models, which are necessarily formulated on a selection of the many processes accompanying tumour evolution. We also tried to provide sufficient motivations for the choices at the basis of the illustrated approaches. The final goal was to reach conclusions of some practical relevance by means of numerical simulations in which the various parameters involved have been taken from the experimental literature.

The theories presented contain some concepts that should always be taken into account when dealing with tumour cords or spheroids. At the same time

other aspects have been ignored, like the analysis and influence of stresses whose role can be important. The reason is on one hand to limit the complexity of the models, which nevertheless is still remarkable, and on the other the lack of a convincingly complete constitutive law for the cell-liquid mixture. The very same idea of adopting a two-component scheme cannot be completely satisfactory, although it may be reasonably acceptable for tumour cords that do not seem to develop a substantial extracellular matrix. Because of the importance of the subject and the intrinsic complexity of tumours, we believe that when attempting to formulate a mathematical model, particularly in the critical field of treatments, one should explicitly declare its limits of applicability.

That said, we can also affirm that the results we have illustrated have implications of practical interest. This refers in particular to the conclusions about the effectiveness of splitting the dose in chemotherapy and the different scenario that is offered when one poses the same question for radiation treatments. The description of how monoclonal antibodies are absorbed in a cord looks also of practical relevance. Model predictions, although substantially qualitative, appear sufficiently precise to suggest experimental work aimed at their confirmation.

## References


[1] Anderson, A.R.: A hybrid mathematical model of solid tumour invasion: the importance of cell adhesion. Math. Med. Biol., **22**, 163–86 (2005).

[2] Araujo, R.P., McElwain, D.L.S.: New insights into vascular collapse and growth dynamics in solid tumors. J. Theor. Biol., **228**, 335–46 (2004).

[3] Araujo, R.P., McElwain, D.L.S.: A history of the study of solid tumour growth: the contribution of mathematical modelling. Bull. Math. Biol., **66**, 1039–91 (2004).

[4] Berinstein, N.L.: Biological therapy of cancer. In: Tannock, I.F., Hill, R.P. (eds) The Basic Science of Oncology. McGraw-Hill, New York, pp. 420–42 (1998).

[5] Bertuzzi, A., Gandolfi, A.: Cell kinetics in a tumour cord. J. Theor. Biol., **204**, 587–99 (2000).

[6] Bertuzzi, A., Fasano, A., Gandolfi, A., Marangi, D.: Cell kinetics in tumour cords studied by a model with variable cell cycle length. Math. Biosci., **177/178**, 103–25 (2002).

[7] Bertuzzi, A., d'Onofrio, A., Fasano, A., Gandolfi, A.: Regression and regrowth of tumour cords following single-dose anticancer treatment. Bull. Math. Biol., **65**, 903–31 (2003).

[8] Bertuzzi, A., Fasano, A., Gandolfi, A.: A free boundary problem with unilateral constraints describing the evolution of a tumour cord under the influence of cell killing agents. SIAM J. Math. Anal., **36**, 882–915 (2004).

[9] Bertuzzi, A., Fasano, A., Gandolfi, A.: A mathematical model for tumor cords incorporating the flow of interstitial fluid. Math. Mod. Meth. Appl. Sci., **15**, 1735–77 (2005).

[10] Bertuzzi, A., Fasano, A., Gandolfi, A., Sinisgalli, S.: Interstitial pressure and extracellular fluid motion in tumor cords. Math. Biosci. Engng., **2**, 445–60 (2005).

[11] Bertuzzi, A., Fasano, A., Gandolfi, A., Sinisgalli, C.: Cell resensitization after delivery of a cycle-specific anticancer drug and effect of dose splitting: learning from tumour cords. J. Theor. Biol., **244**, 388–99 (2007).

[12] Bertuzzi, A., Fasano, A., Gandolfi, A., Sinisgalli, C.: The transport of specific monoclonal antibodies in tumour cords. In: Aletti, G., Burger, M., Micheletti, A., Morale, D. (eds) Math Everywhere: Deterministic and Stochastic Modelling in Biomedicine, Economics and Industry. Springer-Verlag, Berlin Heidelberg, pp. 151–64 (2007).

[13] Bertuzzi, A., Fasano, A., Gandolfi, A., Sinisgalli, C.: Reoxygenation and split-dose response to radiation in tumours with Krogh-like vasculature. Bull. Math. Biol., submitted.

[14] Brenner, D.J., Hlatky, L.R., Hahnfeldt, P.J., Hall, E.J., Sachs, R.K.: A convenient extension of the linear-quadratic model to include redistribution and reoxygenation. Int. J. Radiat. Oncol. Biol. Phys., **32**, 379–90 (1995).

[15] Breward, C.J.W., Byrne, H.M., Lewis, C.E.: A multiphase model describing vascular tumour growth. Bull. Math. Biol., **65**, 609–40 (2003).

[16] Bru, A., Albertos, S., Luis Subiza, J., Garcia-Asenjo, J.L., Bru, I.: The universal dynamics of tumor growth. Biophys. J., **85**, 2948–61 (2003).

[17] Byrne, H.M.: Modelling avascular tumour growth. In: Preziosi, L. (ed) Cancer Modelling and Simulation. Chapman & Hall/CRC, Boca Raton, pp. 75–120 (2003).

[18] Byrne, H.M., Preziosi, L.: Modelling solid tumour growth using the theory of mixtures. Math. Med. Biol., **20**, 341–66 (2003).

[19] Casciari, J.J., Sotirchos, S.V., Sutherland, R.M.: Mathematical modelling of microenvironment and growth in EMT6/Ro multicellular tumour spheroids. Cell. Prolif., **25**, 1–22 (1992).

[20] Chaplain, M.A., Graziano, L., Preziosi, L.: Mathematical modelling of the loss of tissue compression responsiveness and its role in solid tumour development. Math. Med. Biol., **23**, 197–229 (2006).

[21] Crokart N., Jordan, B.F., Baudelet, C., Ansiaux, R., Sonveaux, P., Grégoire, V., Beghein, N., DeWever, J., Bouzin, C., Feron, O., Gallez, B.: Early reoxygenation in tumors after irradiation: determining factors and consequences for radiotherapy regimens using daily multiple fractions. Int. J. Radiat. Oncol. Biol. Phys., **63**, 901–10 (2005).

[22] Curtis, S.B.: Lethal and potentially lethal lesions induced by radiations - a unified repair model. Radiat. Res., **106**, 252–70 (1986).

[23] Dyson, J., Villella-Bressan, R., Webb, G.F.: The evolution of a tumor cord cell population. Comm. Pure Appl. Anal., **3**, 331–52 (2004).

[24] Fasano, A., Bertuzzi, A., Gandolfi, A.: Mathematical modelling of tumour growth and treatment. In: Quarteroni, A., Formaggia, L.,

Veneziani, A. (eds) Complex Systems in Biomedicine. Springer-Verlag Italia, Milano, pp. 71–108 (2006).

[25] Ferreira Junior, S.C., Matrins, M.L., Vilela, M.J.: The reaction diffusion model for the growth of avascular tumors. Phys. Rev. E, **65**, 1–8 (2002).

[26] Friedman, A., Reitich, F.: Analysis of a mathematical model for the growth of tumors. J. Math. Biol., **38**, 262–84 (1999).

[27] Friedman, A., Tao, Y.: Analysis of a model of a virus that replicates selectively in tumor cells. J. Math. Biol., **47**, 391–423 (2003).

[28] Fujimori, K., Covell, D.G., Fletcher, J.E., Weinstein, J.N.: Modeling analysis of the global and microscopic distribution of immunoglobulin G, $F(ab')_2$, and Fab in tumors. Cancer Res., **49**, 5656–63 (1989).

[29] Hirst, D.G., Denekamp, J.: Tumour cell proliferation in relation to the vasculature. Cell Tissue Kinet., **12**, 31–42 (1979).

[30] Hlatky, L.R., Hahnfeldt, P., Sachs, R.K.: Influence of time-dependent stochastic heterogeneity on the radiation response of a cell population. Math. Biosci., **122**, 201–20 (1994).

[31] Jain, R.K.: Normalization of tumor vasculature: an emerging concept in antiangiogenic therapy. Science, **307**, 58–62 (2005).

[32] Krogh, A.: The number and distribution of capillaries in muscles with calculations of the oxygen pressure head necessary to supply the tissue. J. Physiol., **52**, 409–15 (1919).

[33] Moore, J.V., Hasleton, P.S., Buckley, C.H.: Tumour cords in 52 human bronchial and cervical squamous cell carcinomas: inferences for their cellular kinetics and radiobiology. Br. J. Cancer, **51**, 407–13 (1985).

[34] Mueller-Klieser, W.: Multicellular spheroids: A review on cellular aggregates in cancer research. J. Cancer Res. Clin. Oncol., **113**, 101–22 (1987).

[35] Smallbone, K., Gavaghan, D.J., Gatenby, R.A., Maini, P.K.: The role of acidity in solid tumour growth and invasion. J. Theor. Biol., **235**, 476–84 (2005).

[36] Tannock, I.F.: The relation between cell proliferation and the vascular system in a transplanted mouse mammary tumour. Br. J. Cancer, **22**, 258–73 (1968).

[37] Thames, H.D.: An 'incomplete-repair' model for survival after fractionated and continuous irradiations. Int. J. Radiat. Biol., **47**, 319–39 (1985).

[38] Venkatasubramanian, R., Henson, M.A., Forbes, N.S.: Incorporating energy metabolism into a growth model of multicellular tumor spheroids. J. Theor. Biol., **242**, 440–53 (2006).

[39] Webb, G.F.: The steady state of a tumor cord cell population. J. Evolut. Equat., **2**, 425–38 (2002).

[40] Wein, L.M., Wu, J.T., Kirn, D.H.: Validation and analysis of a mathematical model of a replication-competent oncolytic virus for cancer

treatment: implications for virus design and delivery. Cancer Res., **63**, 1317–24 (2003).

[41] Wouters, B.G., Brown, J.M.: Cells at intermediate oxygen levels can be more important than the "hypoxic fraction" in determining tumor response to fractionated radiotherapy. Radiat. Res., **147**, 541–50 (1997).